

Combined molecular and atomic potentials for elastic cross sections of electrons scattering off diatomic molecules at intermediate energies

A. Schmalzried^{✉*} and A. Luque^{✉†}

Instituto de Astrofísica de Andalucía, Apartado 3004, 18080 Granada, Spain

N. Lehtinen^{✉‡}

Birkeland Center for Space Science, University of Bergen, N-5020 Bergen, Norway

 (Received 24 December 2021; revised 18 July 2022; accepted 23 August 2022; published 29 September 2022)

A simple model is proposed to compute electron-diatom molecule elastic differential cross sections at intermediate energies within the framework of an analytical local optical potential. In a spherical harmonic expansion of the molecular potential we treat the isotropic term with the partial-wave decomposition and apply the independent atom model (IAM) on all higher orders. This model is seen to properly converge to the IAM at high energies, while bringing significant improvement at lower energies. We compare the results with a well-tested program called ELSEPA, tailored for high-energy electron-atom scattering and address its further extension to molecules with the method proposed. The simplicity of the calculations and the encouraging agreement in shape with experimental data could promote attractiveness among plasma physics simulations in need of coherent and well-resolved differential cross sections.

DOI: [10.1103/PhysRevA.106.032813](https://doi.org/10.1103/PhysRevA.106.032813)

I. INTRODUCTION

The importance of (differential) cross sections for electron-molecule collisions can be found in many applications of plasma physics, such as Monte Carlo simulations of electron swarms in gases [1], atmospheric physics [2], electric discharges [3], gas lasers [4], runaway mechanisms [5], plasma catalysers. They can either be obtained from experimental measurements [6–8] or quantum calculations [9–12].

Lately, free online databases [13,14] have been set up to readily provide cross sections from various sources. Additionally, freely available codes such as ELSEPA [15,16] or UKRmol [17] enable the generation of elastic differential cross sections (DCS) for all atoms and many polyatomic molecules in the complementary domains of high-energy and low-energy scattering.

When it comes to generating a database of good quality and resolution, there arise some difficulties. Experimental databases can be sparse, lack data at both angular extremes and can be controversial on occasions due to different methods used for calibration, angular allowance aperture, precision in energy and angle [18]. Codes on the other hand can consistently generate DCS but might take considerable time and inevitably are limited to a range of validity. For instance, ELSEPA [15,16], works remarkably well for molecules in the independent atom model [19] impacted by electrons of more than 100 eV, but is less accurate in the intermediate range 10–100 eV, where typically, the DCS

gradually evolves from a roughly symmetric cusp at 90°, to a forward angular distribution. On the other end, UKRmol (and its perfected distributions for industrial applications QUANTEMOL-N [20]-EC [21]), covers all cross sections for low-energy electron-molecule interactions but is computationally costly and requires more user experience. This leaves a gap in the intermediate energy range, which is known to be fillable with variational [22,23] or close-coupling [24–26] methods.

Alternatively, there have been some publications centered on a considerably simpler analytical [27,28] description of the DCS or a partial-wave [29–31] analysis applied to an analytical optical potential, which yielded reasonable results over different ranges of validity. So far, accuracy in producing outputs has been pushed jointly with the level of sophistication while using approximations to abridge computational costs where appropriate.

We propose here instead to withdraw from complexity, and give practical recommendations on how to obtain accurate DCS, yet using the simplest tools and models available. We show how replacing the zeroth (isotropic) interference term in the independent atom model by a (molecular) partial-wave scattering amplitude can considerably extend the independent atom model's range of applicability toward the lower end of intermediate energies. The DCS is reconstructed based on its analogous decomposition in the first Born approximation. For this, we construct an optical potential taken from the simplest models [32–35] available for electron-molecule scattering. The aim is to provide the community of plasma physics with the tools necessary to generate DCS with relative ease. This work is partly based on Salvat *et al.*'s [28] simple model for electron-atom scattering, which we extended to apply on diatomic molecules.

*aschmalz@iaa.es

†aluque@iaa.es

‡nikolai.lehtinen@uib.no

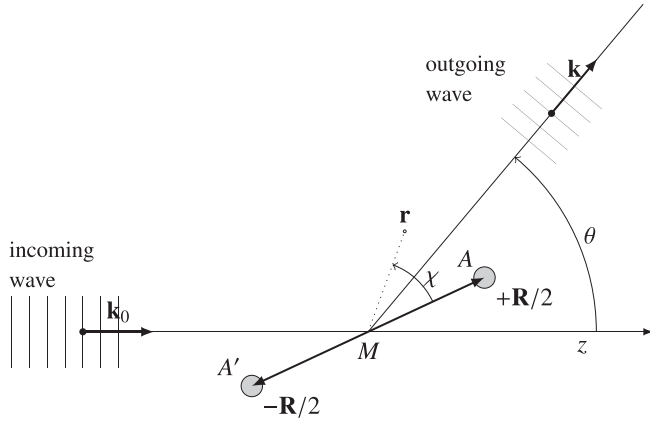


FIG. 1. The scattering of an electron about a diatomic molecule of internuclear distance R viewed from a fixed (laboratory) reference frame with the z axis aligned with the incoming direction

The sections are structured as follows: a short introduction to potential scattering theory; a presentation of the optical potential employed; a description of three ingredients featured in our approach, namely potential harmonic expansion, independent atom model (IAM), and partial-wave decompositions; and finally results with suitable comparisons in different energy domains. Due to their notable presence in (atmospheric) gaseous electronics, we focus on H_2 , N_2 , and O_2 in particular, and briefly discuss NO and CO.

II. POTENTIAL SCATTERING

The potential scattering formalism, adequate for describing weakly inelastic electron-molecule collisions [23,24,36,37], relies upon the Schrödinger equation for the electron's static wave function $\psi(\mathbf{r})$ evolving in a space occupied by an effective interaction potential $V(\mathbf{r}, \mathbf{R})$ traditionally centered on the diatomic molecule's center of mass assumed, in our cases, to lie at the midpoint of the interatomic separation \mathbf{R} :

$$-\frac{\hbar^2}{2\mu}\Delta\psi(\mathbf{r}) + V(\mathbf{r}, \mathbf{R})\psi(\mathbf{r}) = E\psi(\mathbf{r}). \quad (1)$$

The mass of the target M_t , usually considered infinitely large [37, p. 220] compared to the electron m_e , can optionally be roughly accounted for via the reduced mass of the system [38]: $\mu = m_e M_t / (M_t + m_e) \cong m_e$. In (1), E represents the asymptotic kinetic energy of the electron $E \equiv \hbar^2 |\mathbf{k}|^2 / 2m_e$.

The boundary condition applied to the wave function [39] relates the incident and outgoing plane waves of respective wave vectors \mathbf{k}_0 and \mathbf{k} :

$$\psi(\mathbf{r}) \xrightarrow{r \rightarrow \infty} \exp(i\mathbf{k}_0 \cdot \mathbf{r}) - \frac{2\mu}{\hbar^2} \frac{\exp(ikr)}{4\pi r} \times \int_{\mathbf{r}'} e^{-i\mathbf{k} \cdot \mathbf{r}'} V(\mathbf{r}', \mathbf{R}) \psi(\mathbf{r}') d^3 \mathbf{r}'. \quad (2)$$

The overall scattering process described can be visualized in Fig. 1.

For vibrationally elastic collisions at intermediate energies, one can additionally assume that the electron's kinetic energy greatly surpasses the rotational excitations of the molecule

leading to two simplifications: the neglect of the energy loss [40] $|\mathbf{k}_0| \approx |\mathbf{k}|$ and the adiabatic [37,41,42] (or impulse) approximation in which the molecule remains fixed in space during the entire collision process.

For a linear molecule in a Σ_g state (molecular electronic orbital and spin momenta with null projection on the internuclear axis) all rotational states of excitation can be described with spherical harmonics $Y_J^M(\hat{\mathbf{R}})$ of the molecular axis $\hat{\mathbf{R}}$ with J, M quanta for the rotational momentum and its projection (on the z axis of the reference frame on Fig. 1). The scattering amplitude for an excitation $J_0, M_0 \rightarrow J, M$ is given by [40, p. 117]:

$$f(\mathbf{k}JM \leftarrow \mathbf{k}_0 J_0 M_0) = -\frac{2\mu}{4\pi\hbar^2} \int_{\hat{\mathbf{R}}} \int_{\mathbf{r}'} Y_J^{M*}(\hat{\mathbf{R}}) e^{-i\mathbf{k} \cdot \mathbf{r}'} V(\mathbf{r}', \mathbf{R}) \times \psi_{\mathbf{R}}(\mathbf{r}') Y_{J_0}^{M_0}(\hat{\mathbf{R}}) d^3 \mathbf{r}' d\hat{\mathbf{R}}. \quad (3)$$

The parametric dependence of the wave function $\psi_{\mathbf{R}}$ upon \mathbf{R} makes the integration cumbersome [11]. Nevertheless, a way around exists by considering the first-order solution of the iterative equation (2) known as the (first) Born approximation [40, p. 116]. It effectively replaces the full wave function by the incident plane wave in (2)'s integrand:

$$\tilde{f}(\mathbf{k}JM \leftarrow \mathbf{k}_0 J_0 M_0) = -\frac{2\mu}{4\pi\hbar^2} \int_{\hat{\mathbf{R}}} \int_{\mathbf{r}'} Y_J^{M*}(\hat{\mathbf{R}}) e^{-i\mathbf{k} \cdot \mathbf{r}'} V(\mathbf{r}', \mathbf{R}) \times e^{i\mathbf{k}_0 \cdot \mathbf{r}'} Y_{J_0}^{M_0}(\hat{\mathbf{R}}) d^3 \mathbf{r}' d\hat{\mathbf{R}}. \quad (4)$$

Finally, defining the angle θ between \mathbf{k}_0 and \mathbf{k} , one can construct the differential cross section (DCS) from the scattering amplitude in either case, by summing over all final M and averaging over all initial M_0 rotational magnetic states [40].

$$\frac{d\sigma}{d\Omega_{J \leftarrow J_0}} = \frac{k}{k_0} \frac{1}{2J_0 + 1} \sum_{M, M_0} |f(\mathbf{k}JM \leftarrow \mathbf{k}_0 J_0 M_0)|^2. \quad (5)$$

In the rest of the paper, in accordance with the customs of quantum physics, atomic units will be used; in which case $c = \hbar = 1 = e = m_e$, so that kinetic factors in (1)–(4) and electric factors in potentials can be simplified. Units of length and energy are expressed respectively in Bohr's atomic radii $a_0 = 52.918.. \text{ pm}$ and Hartrees $\cong 27.211 \text{ eV}$. In the next section, we present a simple local optical potential for diatomic molecules.

III. OPTICAL POTENTIAL

The effective interaction between the electron and the molecule is approximated by an optical model potential. It is traditionally separated into the static, exchange, polarization, and absorption terms; for each of which we selected and adapted the simplest models available in the literature.

A. Static

Roughly speaking, a diatomic molecule taken from the perspective of an electron scattering at an energy fairly above the ionization threshold can be viewed as an aggregate of two separate atoms [15]. The potential V_s of the atom itself can be approximated by a sum of screened-Coulomb (Yukawa) potentials. Such potentials have the remarkable property [43, pp. 109-110] that their related electronic density ρ (through

TABLE I. Yukawa two-term fits [34] to Dirac-Hartree-Fock-Slater calculated atomic potentials. The parameters are to be used as in Eqs. (6) and (7)

Atom(Z)	H(1)	C(6)	N(7)	O(8)
γ	-184.39	0.1537	0.0996	0.0625
	185.39	0.8463	0.9004	0.9375
λ	2.0027	8.0404	10.812	14.823
	1.9973	1.4913	1.7987	2.0403

Poisson's equation [44, p. 8]) is also uniquely composed of Yukawa-type terms:

$$V_s(r) = -\frac{e^2}{4\pi\epsilon_0}Z \sum_{i=1}^{N_Y} \gamma_i \exp(-\lambda_i r)/r; \quad \text{with } \sum_{i=1}^{N_Y} \gamma_i = 1 \quad (6)$$

$$\rho(r) = \frac{Z}{4\pi} \sum_{i=1}^{N_Y} \frac{\gamma_i}{\lambda_i^2} \exp(-\lambda_i r)/r. \quad (7)$$

The normalization on γ_i coefficients constrains the electronic charge to be equal to the atomic charge number Z . As a consequence of the units chosen, the electric factor for the potential can be omitted and a 4π factor is introduced below Z in the density equation. In the following we will use Salvat *et al.*'s [34] two-term fits for the first-row atoms, for which we give the parameters in Table I. Any deformation of the electron cloud due to the molecular bond, including multipole terms (such as the dipole and the quadrupole) are neglected in the present study.

B. Exchange

The exchange potential represents the possibility [45, §3] that the incident electron replaces and ejects a molecular electron of identical spin. This effect, nonlocal [46, Eq. (2.18)] by nature, can be approximated [33] by a simple local potential in our limiting case of relatively high incident energies:

$$V_{\text{ex}}(\mathbf{r}) \approx \frac{-\pi\rho(\mathbf{r})}{[E - V_s(\mathbf{r})]}. \quad (8)$$

C. Polarization and correlation

The presence of the charged electron induces a deformation on the molecule's electron cloud, which is typically represented by correlation (near-field) and polarization (far-field) potentials. Intuitively, the first part correlates the displacement of the molecular cloud generating a hole [47] around the intruding electron, while the second part emerges from the dipole induced by a displacement of the electronic cloud through its (isotropic) polarizability α_0 , neglecting the non-isotropic part. Both effects can be crudely incorporated into a simple Buckingham [48,49] potential:

$$V_p(r) = -\frac{\alpha_0}{2(r^2 + r_c^2)^2}, \quad (9)$$

$$\text{with } r_c = \sqrt{6E/E_{\text{exc}}}. \quad (10)$$

The cutoff radius r_c is proposed here to match the second order of the asymptotic [32,50] nonadiabatic polarization,

which depends both on an average excitation E_{exc} of the molecule and on the energy E of the incident electron (effectively reducing polarization effects at higher energies). It can be seen as a (third) alternative to the two propositions suggested by Onda [51] about cutting off adiabatic polarization at small ranges and high velocities.

The average excitation E_{exc} has been widely used as a tunable parameter and could even take values higher than the ionization threshold E_{ion} as can be seen in Jain and Baluja [52]. We will follow Onda's [32] suggestion (p. 87, §II.A) and set $E_{\text{exc}} \equiv E_{\text{ion}}$. Lower values would result in flatter DCS at small angles in Fig. 3.

D. Absorption

The last term in the effective optical potential is the absorption potential V_a (sometimes [53] viewed as the imaginary part of the complete polarization potential), which decreases the scattered flux at medium to wide angles due to particle losses into an inelastic channel of electronic excitation. This potential is purely negative imaginary [cf. its use in (13)] and is interpreted as an absorption probability $-2V_a/\hbar$ per unit time [54, §II.B]. We use a widely implemented quasifree local model [35] given by:

$$V_{\text{abs}}(\mathbf{r}, E) = -\frac{\hbar}{2}v_{\text{loc}}(\mathbf{r})\rho(\mathbf{r})\sigma_b(k_F(\rho(\mathbf{r})), E), \quad (11)$$

with the local scattering electron velocity v_{loc} and cross section σ_b for inelastic collisions expressed in terms of the Fermi momentum [35, Eq. (2)] $k_F = \sqrt[3]{3\pi^2\rho(\mathbf{r})}$:

$$v_{\text{loc}} = \sqrt{2(E - V_{\text{se}})/m_e} \quad (12a)$$

$$\sigma_b(k_F, k) = \frac{4\pi}{k^2} \left[\frac{1}{2E_{\text{th}}} - \frac{k'^2 - \frac{3}{5}k_F^2}{(k'^2 - k_F^2)^2} + H \right] : k' > k_{\text{min}}, \quad (12b)$$

$$H = \frac{2}{5k_F^3} \frac{(k_F^2 + k_{\text{min}}^2 - k'^2)^{5/2}}{(k'^2 - k_F^2)^2} : k_F^2 + k_{\text{min}}^2 > k'^2, \quad (12c)$$

$$k_{\text{min}}^2 = k_F^2 + 2E_{\text{th}}, \quad (12d)$$

$$k'^2 = k^2 - 2\left(\frac{1}{r} - \frac{V_s(r)}{Z}\right). \quad (12e)$$

The potential V_{se} in (12a) is simply the sum of static (6) and exchange (8) potentials defined previously. We apply the modification to the original potential introduced by Blanco and García [55] by using k' as defined in (12e), that combines the *local* scattering electron momentum to which the local binding energy of the target electron is subtracted. Without this correction, the absorption potential would be overestimated and produce distortions in the DCS greater than those seen on the right column of Fig. 3.

E. Sum

Originally, the individual atomic potential V_A is simply the sum of electrostatic (s), exchange (e), polarization (p), and absorption (a) potentials. However, since the molecular

polarization is not necessarily equal to the sum of atomic polarizations, we propose to build the total diatomic potential $V(\mathbf{r})$ of atoms A and A' , with two displaced atomic potentials $V_A^{\text{sea}}(\mathbf{r} \pm \mathbf{R}/2)$ without polarisation (V_p crossed in Eq. (13)) derived from their atomic density distributions $\rho(\mathbf{r} \pm \mathbf{R}/2)$, and a total molecular polarization centered on the internuclear midpoint M :

$$V_A^{\text{sea}}(r) = V_s(r) + V_{\text{ex}}(r) + \cancel{V_{\text{p}}} + iV_{\text{abs}}(r), \quad (13)$$

$$V(\mathbf{r}) = V_A^{\text{sea}}\left(\left|\mathbf{r} - \frac{\mathbf{R}}{2}\right|\right) + V_{A'}^{\text{sea}}\left(\left|\mathbf{r} + \frac{\mathbf{R}}{2}\right|\right) + V_p(r). \quad (14)$$

As we will see later in Sec. IV D, it will be very useful to isolate the isotropic term in the molecular potential through a Legendre polynomial expansion in the cosine of χ (see Fig. 1), the angle between \mathbf{r} and \mathbf{R} :

$$V(\mathbf{r}) = V_0(r) + \sum_{l=1}^{\infty} V_l(r) P_l(\cos \chi), \quad (15)$$

$$V_0(r) \equiv V_{A0}^{\text{sea}}(r) + V_{A'0}^{\text{sea}}(r) + V_p(r). \quad (16)$$

For simplicity, we will only consider the explicit expression for V_0 . The higher-order terms will be implicitly treated via the independent atom approximation seen below. The spherical averages of the decentered atomic potentials V_{A0}^{sea} and $V_{A'0}^{\text{sea}}$ are calculated as follows. For the static part, the isotropic component of a decentered Yukawa potential can be obtained from the first term of its addition theorem [56, p. 107]:

$$\frac{Z}{2} \int_{-1}^{+1} \frac{\exp(-\lambda|\mathbf{r} \pm \mathbf{R}/2|)}{|\mathbf{r} \pm \mathbf{R}/2|} d\xi = Z \frac{\sinh(\lambda r_{<})}{\lambda r_{<}} \frac{\exp(-\lambda r_{>})}{r_{>}}. \quad (17)$$

The integral in (17) operates on $\xi = \cos \chi$ and $r_{<}$ ($r_{>}$) correspond to the lesser (greater) among r and $R/2$.

Unfortunately, the exchange and absorption potentials V^{ea} do not lend themselves to a similarly straightforward expression for their spherically symmetric term. The averaging ought to be made numerically as:

$$V_0^{\text{ea}}(r) = \frac{1}{2} \int_{-1}^1 \left[V_A^{\text{ea}}\left(\sqrt{r^2 + \frac{R^2}{4} - rR\xi}\right) + V_{A'}^{\text{ea}}\left(\sqrt{r^2 + \frac{R^2}{4} + rR\xi}\right) \right] d\xi. \quad (18)$$

Nevertheless, we can first attempt to approximate V_0^{ea} by assuming that the nonlinear density-dependent part of the exchange and absorption potentials is sufficiently small so that their spherical average can be matched to that of the molecular density ρ_0 . The error committed thus at small radii was checked to lie within 15% and becomes negligible for $r \geq R/2$. At intermediate energies, the exchange and absorption terms are of minor importance compared to the static potential and the resulting DCS should not be significantly affected. In the results section, we assess the validity and

TABLE II. Molecular parameters: R : internuclear separation [69], Table 2.1; α_0 : static dipole polarizability [69], Table 4.6 [for Eq. (9)]; E_{ion} : ionization energy [69], Table 3.3 [for Eq. (10)]; E_{th} : threshold (electronic) excitation energy [70] [for Eq. (11)]. For O_2 we distinguish the first optically allowed state (from the first valence state in brackets), as discussed below.

	H_2	N_2	O_2	CO	NO
R (a ₀)	1.4011	2.0743	2.281	2.1322	2.1746
α_0 (a ₀ ³)	5.426	11.74	10.67	13.15	11.47
E_{ion} (eV)	15.426	15.581	12.07	14.014	9.264
E_{th} (eV)	6.9	6.17	7 (0.977)	6.006	5.48

limitations of this additional simplification. The approximate expression for V_0 (16) now becomes:

$$V_0(r) \approx V_{s0}(r) - \frac{\pi \rho_0(r)}{E - V_{s0}(r)} - \frac{\alpha_0}{2(r^2 + r_c^2)^2} - i \frac{v_{\text{loc}}}{2} \rho_0(r) \sigma_b(k_F(\rho_0(r)), E); \quad (19)$$

$$V_{s0}(r) = - \sum_{A,A'} Z \sum_{i=1}^{N_Y} \gamma_i \frac{\sinh(\lambda_i r_{<})}{\lambda_i r_{<}} \frac{\exp(-\lambda_i r_{>})}{r_{>}}, \quad (20)$$

$$\rho_0(r) = \sum_{A,A'} \frac{Z}{4\pi} \sum_{i=1}^{N_Y} \frac{\gamma_i}{\lambda_i^2} \frac{\sinh(\lambda_i r_{<})}{\lambda_i r_{<}} \frac{\exp(-\lambda_i r_{>})}{r_{>}}. \quad (21)$$

For homonuclear molecules, A is simply A' and their sum in (20)–(21) is replaced by a factor 2. The values of the various molecular parameters used in the potentials are regrouped in Table II. In the rest of the paper, the atomic potential V_A^{sea} will be written as V_A implying that static, exchange and absorption contributions are all included. Ultimately, this spherical decomposition of the potential will enable us to perform a simple partial-wave expansion (Sec. IV C) with $V_0(r)$, and use it as input to the IAM (Sec. IV B).

IV. APPROXIMATIONS

A. Potential harmonic expansion

To construct a DCS from the Legendre expansion of the potential in (15), it is most instructive to decompose it in the first Born approximation, which for a rotational excitation from degenerate states J_0 to J combines (4) with (5) to yield [40, p. 119, Eq.(26)]:

$$\frac{d\sigma}{d\Omega_{J \leftarrow J_0}} = \sum_{l=0}^{\infty} \frac{2J+1}{(2l+1)^2} \langle J J_0 0 0 | l 0 \rangle^2 \left| -2 \int r^2 j_l(qr) V_l(r) dr \right|^2, \quad (22)$$

where we introduced the Clebsch-Gordan coefficient $\langle J J_0 0 0 | l 0 \rangle$. The spherical Bessel function of order l , $j_l(qr)$, depends on the norm of the electron momentum change vector: $\mathbf{q} = \mathbf{k} - \mathbf{k}_0$ leading to $q = 2k \sin(\theta/2)$ when the energy loss is neglected.

Except for H_2 , the experimental energy resolution of DCS measurements [57] does not allow us to discern rotational excitation levels. Therefore in practice (even for H_2 unless specified), the DCS ought to be summed over the final

rotational excitation states J , which gives the interesting property of being independent from the initial state J_0 (in the first Born approximation with $k \cong k_0$):

$$\sum_{J=0}^{\infty} \frac{2J+1}{(2l+1)} |\langle JJ_0 00 | l0 \rangle|^2 = 1, \quad (23)$$

$$\frac{d\sigma}{d\Omega} = \sum_{l=0}^{\infty} \frac{1}{2l+1} \left| -2 \int r^2 j_l(qr) V_l(r) dr \right|^2. \quad (24)$$

We can designate each of the terms of (24) inside the modulus brackets as a partial scattering Born amplitude [58] \tilde{f}_l , associated with the potential term V_l of harmonic order l :

$$\tilde{f}_l \equiv -2 \int r^2 j_l(qr) V_l(r) dr. \quad (25)$$

Additionally, if all V_l emerge exclusively from the decomposition of a decentered isotropic potential; as $V_A(|\mathbf{r} \pm \mathbf{R}/2|)$ in (19), we can establish a link [see the derivation of (A7) in Appendix A] to the scattering amplitude \tilde{f}_A of V_A :

$$\tilde{f}_{A_l} = (\mp 1)^l (2l+1) j_l(qR/2) \tilde{f}_A. \quad (26)$$

Furthermore, the simple expressions for the static (6) and polarization (9) potentials lead to analytical results for \tilde{f}_s and \tilde{f}_p given in Appendix B. The use of more accurate scattering amplitudes in (26) will naturally lead to the IAM introduced below (as demonstrated in Appendix A) and will enable to ward off the limitations imposed by the first Born approximation.

B. Independent atom model

To take advantage of our multicentral potential in (14), the expression (26) can be reinjected into (24) to perform the infinite summation of partial amplitudes [throughout (A9) of Appendix A]. The first Born DCS is then only composed of individual contributions \tilde{f}_A , $\tilde{f}_{A'}$, \tilde{f}_M , from each of the isotropic potentials centered at A , A' , and M . In our specific case, \tilde{f}_M is only due to polarization V_p . Nevertheless, we keep the molecular notation M for an easier further generalization.

This result, exact for the first Born approximation, is equivalent to the zeroth order of multiple scattering theory [59] better known as the independent atom approximation [60 Chap. VIII, §3.1]. It can be derived more simply by adding coherently in (27), this time, the exact scattering amplitudes f_A , $f_{A'}$, f_M from each central potential and taking the square modulus. In virtue of (2), the scattering amplitude f_A produced by a potential V_A displaced at $\pm \mathbf{R}/2$ is simply modulated by $\exp(\mp i \mathbf{q} \cdot \mathbf{R}/2)$. Rotational averaging is in this case performed by a normalized angular integral over the nuclear axis $\hat{\mathbf{R}}$.

$$\begin{aligned} \frac{d\sigma_{\text{IAM}}}{d\Omega} &= \frac{1}{4\pi} \int |f_A e^{i\mathbf{q} \cdot \mathbf{R}/2} + f_{A'} e^{-i\mathbf{q} \cdot \mathbf{R}/2} + f_M|^2 d\hat{\mathbf{R}}; \quad (27) \\ &= |f_A|^2 + |f_{A'}|^2 + |f_M|^2 + \frac{1}{4\pi} \int 2\text{Re}[f_A f_{A'}^* e^{i\mathbf{q} \cdot \mathbf{R}}] \\ &\quad + 2\text{Re}[f_M^* (f_A e^{i\mathbf{q} \cdot \mathbf{R}/2} + f_{A'} e^{-i\mathbf{q} \cdot \mathbf{R}/2})] d\hat{\mathbf{R}}, \\ &= |f_A|^2 + |f_{A'}|^2 + |f_M|^2 + 2\text{Re}[f_A f_{A'}^*] \frac{\sin(qR)}{q \cdot R} \end{aligned}$$

$$+ 2\text{Re}[f_M^* (f_A + f_{A'})] \frac{\sin(qR/2)}{qR/2}. \quad (28)$$

To obtain more accurate scattering amplitudes for (28) than those of the first Born approximation, we apply the method of partial waves.

C. Partial wave expansion

For a central potential, Schrödinger's equation (1) can be projected into the eigenset of spherical harmonics for the impacting electron's orbital angular momentum as eigenvalues and solved independently for each order ℓ . Since central potentials conserve the orbital momentum of the projectile, the DCS obtained applies only to pure elastic scattering, the information of which is contained within the phase shift [60, Chap. 2] δ_ℓ for each radial wave function. The latter can be extracted from the asymptotic value ($r \rightarrow \infty$) of the variable phase shift [61] $\delta_\ell(r)$, which is a solution of a first-order differential equation:

$$\frac{d\delta_\ell(r)}{dr} = -2V(r)kr^2 [\cos(\delta_\ell(r))j_\ell(kr) - \sin(\delta_\ell(r))y_\ell(kr)]^2, \quad (29a)$$

$$\delta_\ell(0) = 0. \quad (29b)$$

The spherical Bessel functions of the first j_ℓ and second y_ℓ kind are solutions to the radial free-wave equation (1) with $V \equiv 0$.

The behavior of $j_\ell(kr) \sim (kr)^\ell / (2\ell+1)!!$ for $kr \rightarrow 0$ lessens the short-ranged influence of the potential as ℓ increases, which in turn shrinks the asymptotic value reached by δ_ℓ . Assuming $\delta_\ell \cong 0 \Rightarrow \sin \delta_\ell \cong 0$ and $\cos \delta_\ell \cong 1$ in the right-hand side (RHS) of (29a) reduces to a simple integral [60, V§2.12 and II§2.27]:

$$\tilde{\delta}_\ell = -2k \int_0^\infty V(r) j_\ell^2(kr) r^2 dr. \quad (30)$$

For high values of ℓ , we can thus expect $\lim_{\ell \rightarrow \infty} \tilde{\delta}_\ell = \delta_\ell$ and determine a L_δ beyond which δ_ℓ is assigned the value of $\tilde{\delta}_\ell$. In our case, for energies below 100 eV L_δ varied between 72 and 86 depending on the molecule. Those values decreased with higher energies. The formulas used for computing $\tilde{\delta}_\ell$ for V_s and V_p are given in Appendix B.

The (elastic) scattering amplitude $f(\cos \theta)$ can then be reconstructed from those individual phase shifts δ_ℓ through a series of Legendre polynomials P_ℓ :

$$f(\cos \theta) = \frac{1}{2ik} \sum_{\ell=0}^{\infty} (2\ell+1) [\exp(i2\delta_\ell) - 1] P_\ell(\cos \theta). \quad (31)$$

The equivalent first Born amplitude of the central (atomic or averaged molecular) potential is given as a linear combination [60, V§2, p.89] of $\tilde{\delta}_\ell$, therefore referred to as Born phase shifts:

$$\tilde{f} \equiv \tilde{f}(\cos \theta) = \frac{1}{2ik} \sum_{\ell=0}^{\infty} (2\ell+1) 2i\tilde{\delta}_\ell P_\ell(\cos \theta). \quad (32)$$

In light of the convergence $\lim_{\ell \rightarrow \infty} \tilde{\delta}_\ell = \delta_\ell$, one can truncate the infinite sum of (31) up to L terms and include the remainder through a formula known as the Born closure [23,28] for

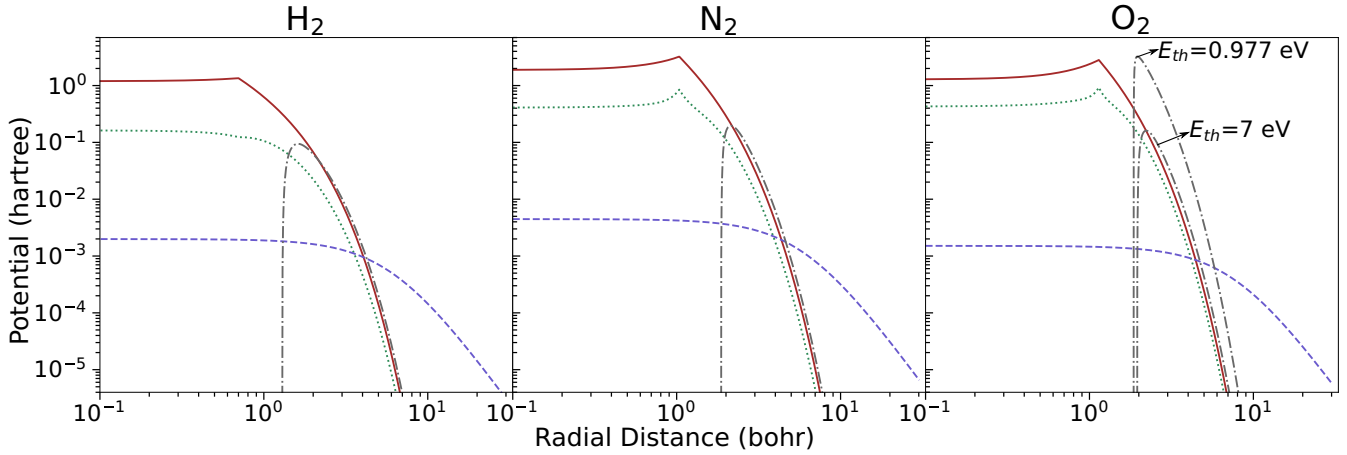


FIG. 2. Isotropic potentials V_0 of H_2 , N_2 , and O_2 from the simple model presented above for an incident electron of 50 eV. Solid brown: Static Yukawa (20), dotted green (\cdots): Exchange (8), dashed purple ($-$): Polarization Buckingham (9), dash-dot gray ($- \cdot -$): Absorption quasifree (11). For O_2 we show how this absorption potential differs for $E_{th} = 0.977$ eV and 7 eV.

the scattering amplitude:

$$\hat{f}(\cos\theta) = \tilde{f} + \frac{1}{2ik} \sum_{\ell=0}^L (2\ell+1)(\exp(i2\delta_\ell) - 1 - 2i\tilde{\delta}_\ell). \quad (33)$$

Here, f stands for either f_A , $f_{A'}$, f_0 , which in our model are all calculated by (31) with $V(r) \equiv V_A, V_{A'}, V_0(r)$ in (29a), and then closed through (33). The upper partial bound L is chosen such that $\delta_\ell < 10^{-6} : \forall \ell > L$ and varies according to the energy taken by the electron. The analytical expressions for \tilde{f} from the (dominant) static and polarization potentials are given in Appendix B.

D. Combined model

Alone, the first Born approximation and the IAM are not expected to yield good results at lower energies. The equations (30) and (32) from the previous section give an indication of the errors committed in the first case. In the second case, (28) should not hold well when the separate potentials $V_A, V_{A'}, V_M$ overlap each other non-negligibly. This is certainly the case for the polarization potential, which is of long range (cf. Fig. 2).

Nevertheless, those two approximations simplify significantly the treatment of electron-molecule scattering. In order to palliate their flaws, our approach consists of three steps.

(i) Use exact partial-wave amplitudes f_i in (26) instead of first Born calculated \tilde{f}_i

(ii) Isolate and calculate the molecular scattering amplitude f_0 from the spherically averaged molecular potential V_0 in (15), which includes the polarization potential V_p (also labeled as V_M in the IAM).

(iii) Subtract the zeroth-order interference term in the IAM and substitute it by the molecular amplitude f_0 .

The first step is analogous to the IAM when one replaces \tilde{f} by f in (A8) to conduce to (28). The second step enables an exact treatment of the interferences arising between the polarization and the first (isotropic) spherical harmonic of the separated atoms. The third step is equivalent to execut-

ing the summation (A9) on spherical Bessel functions from $l = 1$ to ∞ . This procedure, detailed in the Appendix A, leads to our simple model (A10):

$$\frac{1}{C} \frac{d\sigma_{\text{Simple}}}{d\Omega} = |f_0|^2 + |f_A|^2 + |f_{A'}|^2 + 2\text{Re}[f_A f_{A'}^*] \frac{\sin(qR)}{qR} - j_0\left(\frac{qR}{2}\right)^2 |f_A + f_{A'}|^2. \quad (34)$$

Comparing with (28), we see that $|f_0|^2$ now effectively incorporates high-order interferences between the middle term f_M and the isotropic component $f_{A0}, f_{A'0}$ of the two atoms. We show below (top row of Fig. 3) that this procedure enhances the validity of the IAM at lower energies. Notwithstanding, we ought to keep in mind that higher-order interference terms between isotropic and anisotropic terms remain untreated, for (26) might not apply well to partial-wave amplitudes f at lower energies. The forthcoming results section should elucidate this limitation. As the first Born approximation becomes increasingly more valid at higher energies, the simple expression (34) converges toward the IAM (see Fig. 6, bottom panel at 400 eV). This property emerges from the equivalence of (A8) and (A10), and from the linearity of the scattering amplitude (25) with respect to the potentials.

Finally, it is well known that the IAM does not satisfy the optical theorem [62, Eqs. (9)-(11)] for the integrated cross section. For this reason, many attempts [63–65] of renormalizing the DCS based on geometrical arguments were conducted. We retain here the simplest model [65] in which the DCS [LHS of Eq. (34)] is renormalized with a correction factor C :

$$C = 1 - \frac{\sigma_A \sigma_{A'}}{\sigma_A + \sigma_{A'}} \left(\frac{1}{\max(\pi R^2, \sigma_A, \sigma_{A'})} \right) \quad (35)$$

The simplicity of the model presented above may be confusing due to the many approximations taken. To offer a better understanding of the ensuing limitations and their range of validity, we implemented a more advanced potential with:

(i) static density and potential based on Cox and Bonham's [66] six-term Yukawa distribution;

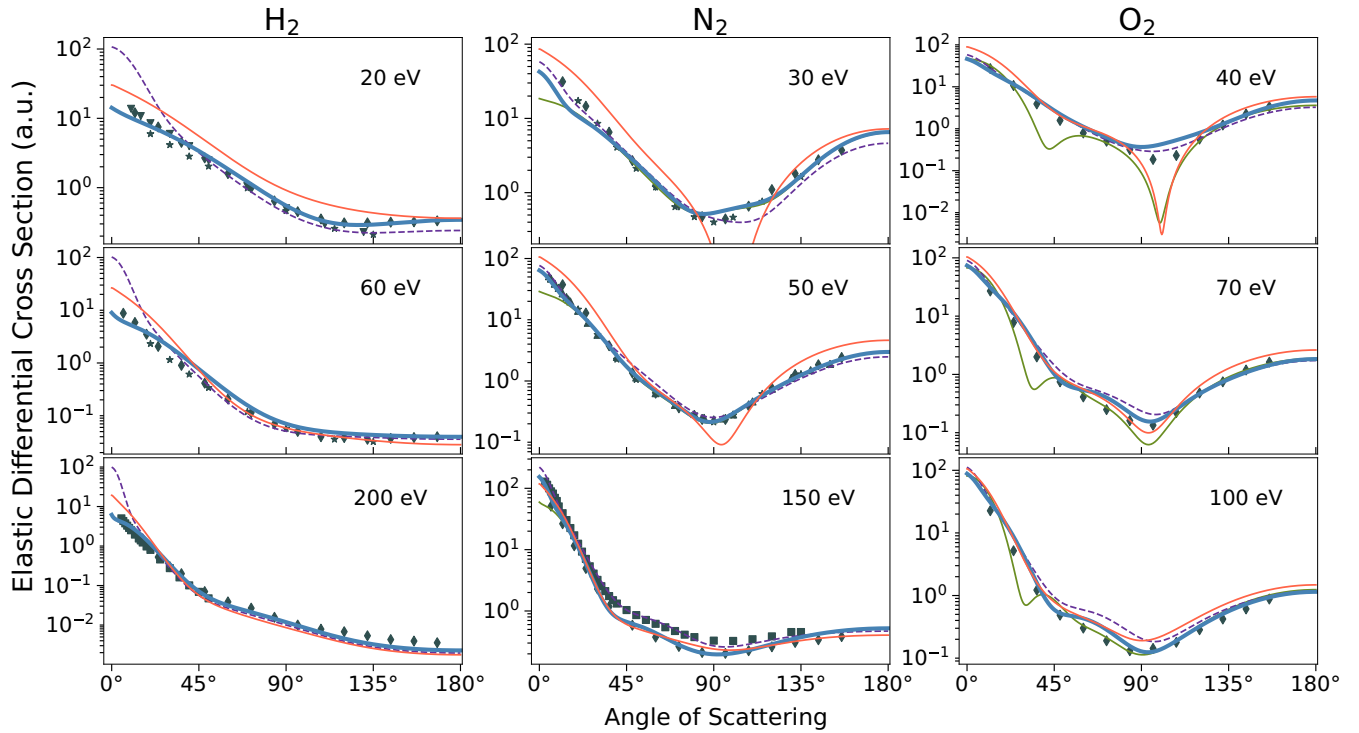


FIG. 3. Differential cross sections (in units of a_0^2/sr) of H_2 , N_2 , and O_2 at various energies. Theoretical calculations: thick blue: our recommended model (see text); solid olive: our simple model represented by Eq. (34); light red: ELSEPA's independent atom model; dashed purple (—): advanced model described at the end of Sec. IV D. Experimental data: H_2 - \star : Srivastava *et al.* [73]; \diamond : Shyn and Sharp [74]; \triangle : Khakoo and Trajmar [75]; ∇ : Muse *et al.* [76]; \square : van Wingerden *et al.* [77]; N_2 - \star : Srivastava *et al.* [78]; \diamond : Shyn and Carignan [79]; \triangle : DuBois and Rudd [80]; \square : Herrmann *et al.* [81]; O_2 - \diamond : Shyn and Sharp [82].

(ii) modified semiclassical exchange potential from Giannurco and Scialla [67, Eq. (18)];

(iii) Buckingham polarization (9) with $r_c = \sqrt{(\frac{3}{2}E_{ion} + 6E)/E_{ion}}$ for the cutoff radius as in Onda and Truhlar [32, Eq. (6)] instead of (10);

(iv) Perdew and Zunger's [68] untruncated correlation potential for atoms as used in Salvat [54, Eq. (7)];

(v) Absorption based on Salvat's [54] Appendix for binary collision cross section as used in ELSEPA.

In order to avoid impairing the accuracy of this advanced potential, we also precisely calculated the spherical average of the nonstatic components following (18) to be used in the molecular potential in (14). Using this last advanced model as a basis for comparison, we would like to demonstrate that depending on the molecule and energy considered, the use of simpler models can still lead to satisfactory results.

V. RESULTS

The simple model we presented earlier (34) is compared to ELSEPA's [15] independent atom model and contrasted with the advanced model that involves more accurate potentials. For each molecule, we then show and recommend the minimal changes to the simple model that enables us to preserve the level of accuracy of the advanced model.

The effect of each molecular parameter, whose value is given in Table II, can be appreciated by looking at the po-

tentials for each molecule in Fig. 2. The peak observed for the static and exchange potentials is located exactly at half the internuclear separation $R/2$. Inclusion of higher-order spherical harmonics would reconstruct the singularity of the decentered Yukawa potential. This peak is weakly pronounced for hydrogen, denoting its relative spherical shape. The highest polarizability α_0 belongs to N_2 , raising the polarization dashed curve at the origin. One can see that the sensitivity upon the exact value of the average excitation energy E_{exc} is effectively low. On the contrary, the absorption is rather sensitive on the threshold energy E_{th} , and is overwhelmingly important for O_2 due to its low-lying excited singlet state.

In Fig. 3, we present elastic differential cross-sections in three different energy ranges for H_2 , N_2 , and O_2 and compare them with experimental data detailed in the figure's caption. One can observe how the agreement of each model depends both on the molecule and the energy chosen.

A. H_2

Hydrogen is by far the least aspherical molecule with a separation radius of only $1.4 a_0$ as opposed to over $2 a_0$ for nitrogen and oxygen. As a consequence, the molecular spherical average analysis yields accurate results even at energies as low as 20 eV. On the other hand, with only two orbiting electrons, local density approximations for the exchange, correlation and absorption potentials do not apply well.

Nonetheless, it was shown [71] that the semiclassical model for exchange fitted best an exact nonlocal treatment of

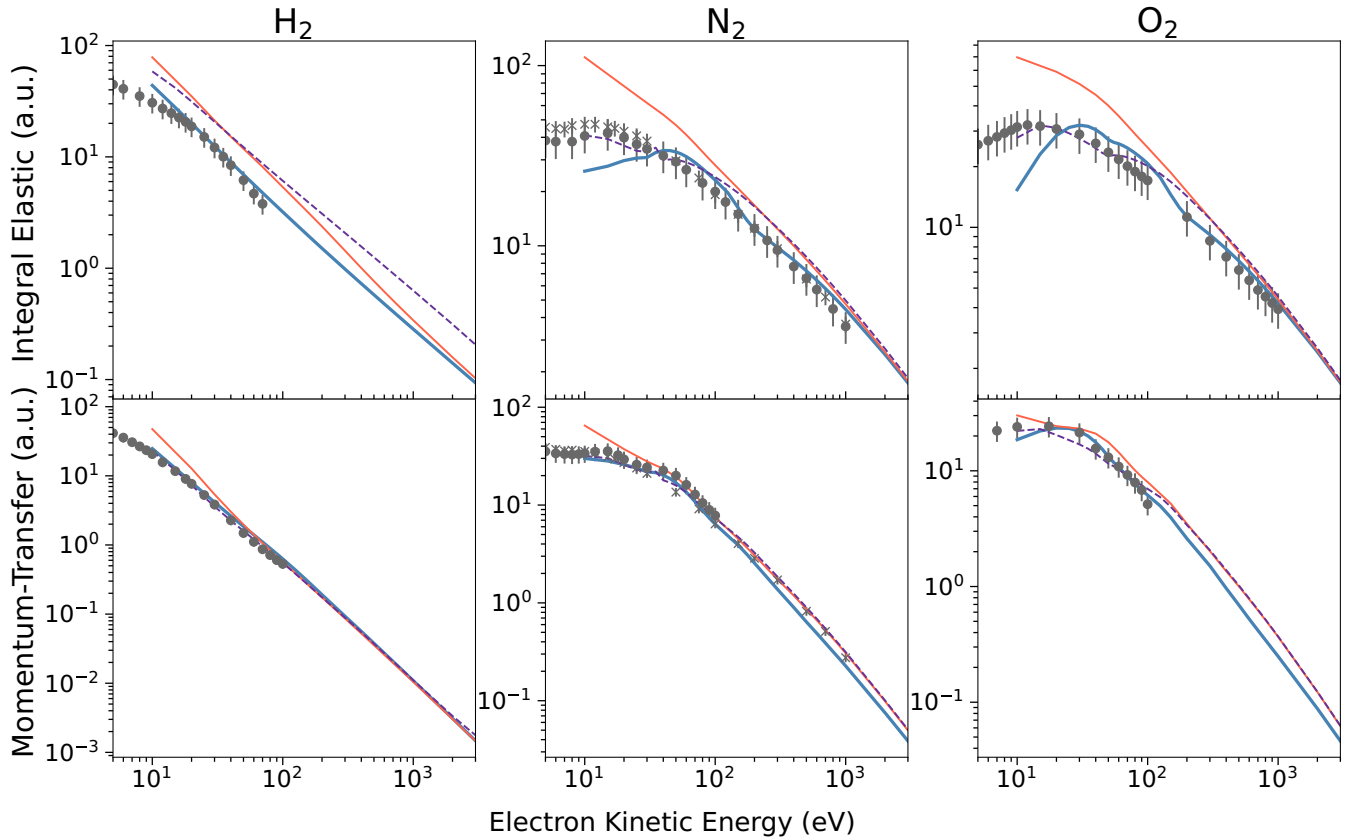


FIG. 4. Integrated (top) and momentum transfer (bottom) elastic cross sections of H_2 , N_2 , and O_2 (in units of a_0^2). Theoretical calculations: thick blue: our recommendation based on our simple model represented by Eq. (34); light red: ELSEPA's independent atom model; dashed purple (—): advanced model described at the end of Sec. IV D. Experimental (Ixcat-2018) databases [14]: \times : Phelps database [85]; \circ : Itikawa database [86–88] with $\pm 20\%$ of uncertainty.

the exchange. The correlation causes the short-range potential to fall less sharply and induces the lump seen at small angle scattering for the advanced model (dashed curve). Next, an absorption potential based on a binary collision cross section with molecular electrons modeled as a free electron gas, such as the ones presented here, is not relevant for hydrogen. Previous studies [42,72] on H_2 using potential scattering accounted for the static-exchange-polarization trio. There, the polarization term treats rigorously the higher-order interactions of the scattering electron with molecular electrons.

For purely illustrative purposes, the light red and purple dashed curves on the left column of Fig. 3 show how the unsuitable inclusion of correlation and absorption for H_2 is, respectively, characterized by an overestimation (lump) at small angles and a minor underestimation at large angles. The effect of absorption is reduced due to the relatively high excitation threshold of H_2 and low molecular electronic density. This underlines the dominance of the static potential at non-small scattering angles.

Remarkably, our simple static-exchange-polarization potential represented by the thick blue curve on Fig. 3 covers well a wide range of energies, which we interpret as resulting from the relative simplicity of the hydrogen molecule. Because the molecular contribution to the DCS prevails over the IAM at intermediate energies, *no correction* factor was used ($C \equiv 1$) in any of the DCS and CS for H_2 on Figs. 3 and 4. In this case, we recommend directly using our simple model

which is why the solid-olive curve for H_2 is not visible on Fig. 3.

B. N_2

For nitrogen, we observe the typical dip (also present for oxygen) around 20–40 eV at intermediate angles due to the IAM interference term $\sin(qR)/qR$ passing through a minimum around $qR \approx \frac{3}{2}\pi$ that coincides with the cusp in the atomic scattering amplitude around 90° for $R \simeq 2a_0$. This artifact can be bypassed with the molecular scattering amplitude, albeit with a slight overestimation instead. On the top middle graph of Fig. 3, we compare four different models. The dashed line represents the advanced model with an accurate treatment of the spherical averaging.

Here we can best assess the error committed by the simplification taken in (19) by naively replacing ρ by ρ_0 . At higher energies, this simplification is acquitted by two effects. First, the exchange potential becomes effectively more linear as can be seen in (8). Second, absorption does principally affect the DCS at larger angles [23,54, §V]. By contrast, for higher energies, the contribution of the molecular potential V_0 is only relevant at small angles. For this reason, above roughly 50 eV this simplification becomes acceptable.

At lower energies, a close-coupled study [23,26] reveals that the coupling between different partial waves becomes important for the first orders. This implies that one has to

include more spherical harmonics in the molecular potential (15) and abandon the zero-order interference given by the IAM.

Interestingly, the main difference at higher energies (middle and bottom rows in Fig. 3) between our advanced and simple models builds up at small-angle scattering due to a too weak polarization-correlation potential at small radii. The inclusion of a more accurate potential [68 Appendix C] straightens the forward scattering for N_2 and O_2 for the advanced model given by the dashed curve. Thus the blue curve showing our recommendation just adds this correlation [54, §A, Eq. (7)] potential to our simple model in (13).

C. O_2

The most interesting discussion emerges from the results for oxygen. Its first excited singlet state is not far above the ground triplet state, leaving a very small electronic excitation threshold at 0.977 eV. As a result, the quasifree absorption potential in (11) is greatly overestimated and spoils low-order phase shifts for $\ell = 2..8$, by inducing a considerable rotation in the complex plane through their differential equation (29a). The two drops around 40° and 100° of the simple model result from this excessive absorption. There are two ways to amend this inaccuracy. As suggested by Blanco and García [55, §II.C], one ought to take the first optically allowed excitation state for E_{th} , which in the case of O_2 lies at the foot of the Schumann-Runge continuum [83,84, §3.8,§1] that is set at 7 eV. Alternatively, the more accurate albeit cumbersome potential model [54] used by ELSEPA presents a lower sensitivity to the threshold energy and reproduces well the results for $E_{th} = 0.977$ eV.

Furthermore, there is an ambiguity in the selection of lower excitation threshold when representing the potential of an atom within the molecule. As can be seen on Fig. 3, especially for O_2 , the two absorption potentials (quasifree [35,55] of Eqs. (11)–(12) and ELSEPA [54, §B.(12)]) do not yield equivalent DCS at intermediate energies. The interpretation of the minimal threshold depends on the model used. For the other molecules, N_2 , CO, and NO, their lowest electronic state is not isolated from higher excited states as for O_2 , which we surmise is why it is not required, in those cases, to select a higher electronic threshold E_{th} to be used in the quasifree model (11).

D. Integral and momentum-transfer cross sections

An overview of the performance of various models can be better assessed by looking at their integrated (σ) and momentum-transfer (σ_m) cross sections in Fig. 4. The latter are obtained from the DCS through an integration in the angular solid space:

$$\sigma = 2\pi \int_0^\pi \frac{d\sigma}{d\Omega}(\cos\theta) \sin\theta d\theta, \quad (36)$$

$$\sigma_m = 2\pi \int_0^\pi \frac{d\sigma}{d\Omega}(\cos\theta)(1 - \cos\theta) \sin\theta d\theta. \quad (37)$$

The earlier analysis conducted upon the DCS in Fig. 3 is restated in Fig. 4. For hydrogen, the simple model presented performs best in generating elastic cross sections in the energy range 10 eV–1 keV, due to its short internuclear separation. ELSEPA's results converge to our model beyond 100 eV for

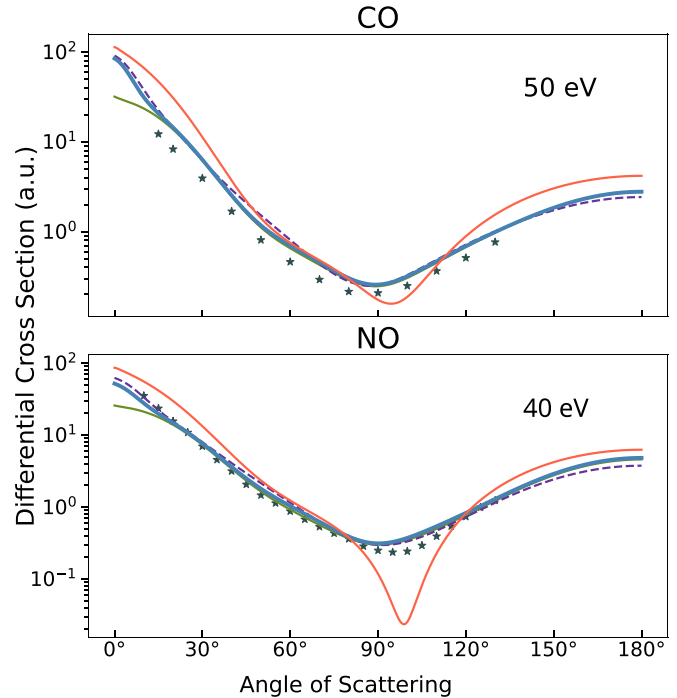


FIG. 5. Differential cross sections applied to heterogeneous molecules: CO and NO. Theoretical calculations: thick blue: our recommended model (see text); solid olive: our simple model represented by Eq. (34); light red: ELSEPA's independent atom model; dashed purple (–): advanced model described at the end of Sec. IV D. Experimental data: CO - *; Tanaka *et al.* [90]; NO - *; Mojarrabi *et al.* [91].

the momentum transfer and beyond 2 keV for the integrated cross section. The disagreement at small-angle scattering of the advanced model seen on Fig. 3, left, is responsible for the systematic bias in the CS on the top right graph of Fig. 4. However, when switching to the momentum transfer, this discrepancy is washed out through the $(1 - \cos\theta)$ factor in the formula (37). For nitrogen and oxygen, the correction factor C from (35) is essential for obtaining a good agreement with the integrated DCS. Otherwise, the curves would present a systematic overestimation similar to the one given by the IAM with ELSEPA on the top row of Fig. 4.

An overall agreement is reached at higher energies beyond 200 eV. As expected, ELSEPA and our advanced model converge since they rely upon a similar potential. However, a shift in the momentum transfer persists on the bottom row of Fig. 4. This denotes the fact that scattering at large angles differs in our simple model. Again, this is induced by the two different modeling approaches to the absorption potential. Experimental data is lacking above 100 eV to help in settling this issue.

E. NO and CO

Finally, the model can also be applied to heterogeneous diatomic molecules, with selected examples shown in Fig. 5 for CO and NO. The conclusions are similar: the polarization is underestimated and needs to be supplemented with the correlation potential from the advanced model, the correction factor C greatly reduces the systematic bias at lower

energies, and the effect of $|f_0|^2$ in Eq. (34) introduces a slight overestimation at intermediate angles (best seen for NO) whereas ELSEPA's results present an underestimation dip around 100° . In addition, it is possible that CO and NO's permanent dipole [40,80,89] have a small contribution in the forward scattering.

VI. DISCUSSION

We presented a methodology for computing electron elastic scattering cross sections with diatomic molecules that connects the independent atom model (IAM) valid at high energies to the partial-wave shifts of a molecular potential apt at lower energies. To connect those two approaches, we borrowed the deconstruction of the IAM as a sum of first Born amplitudes and proposed to replace the latter by the more accurate amplitudes coming from the partial-wave analysis.

The resulting DCS palliate the shortcomings of the IAM at lower energies by removing dips caused by an insufficient description of higher interatomic interference terms [22]. The agreement in shape can be considered satisfactory even down to 30 eV, which we consider the validity range of our method. Nevertheless, due to the violation of the optical theorem by the IAM [62, Eq. (9)-(11)], our DCS at lower energies tend to overestimate scattering over all angles and require a screening correction factor [65] as defined by (35). Also, at below 30 eV, our DCS gradually flattens the cusp observed experimentally at intermediate angles.

Previous studies presented different ways [92,94] to treat atomic-centered potentials and long-range molecular potentials [93] through the IAM augmented with multiple intra-molecular scattering corrections [59,95,96]. The analysis revealed that higher-order terms become important [22, §3] below 60 eV and the convergence is slow [62,97 Fig. 7, pp. 1918-1919]. With the present methodology, one can significantly incorporate the effects of intramolecular scattering through a partial-wave analysis [yielding $|f_0|^2$ in Eq. (34)] on the isotropic molecular potential V_0 . In Fig. 6, we compare our model with the screened IAM model of Blanco and García [29] and higher-order IAM of Hayashi and Kuchitsu [59] as implemented by Jain and Tayal [93]. Also represented are the separate contributions of the molecular isotropic term $|f_0|^2$ from the remaining interatomic interferences terms of Eqs. (34) or (A10). We see that while all models converge at higher energies where the Born approximation becomes more acceptable, the situation is different at lower energies.

Of particular interest is that the higher-order IAM (in orange), through its corrections of single and double scattering interference terms, gives an overall good agreement without requiring any rescaling with a screening factor C as defined by (35). Since the present model is a resummation of the multiple IAM but limited to the zero-order interference, further improvement could be sought by incorporating higher-order interferences from multiple scattering into (34). Without this extension, by using a separate treatment of the isotropic molecular (V_0) and the atomic ($V_A, V_{A'}$) potentials, our model still brings an improvement on the screened IAM at lower energies and simplifies the treatment of higher-order IAM.

Looking toward the low-energy limit, at least three limitations were identified that invalidate the use of our simple

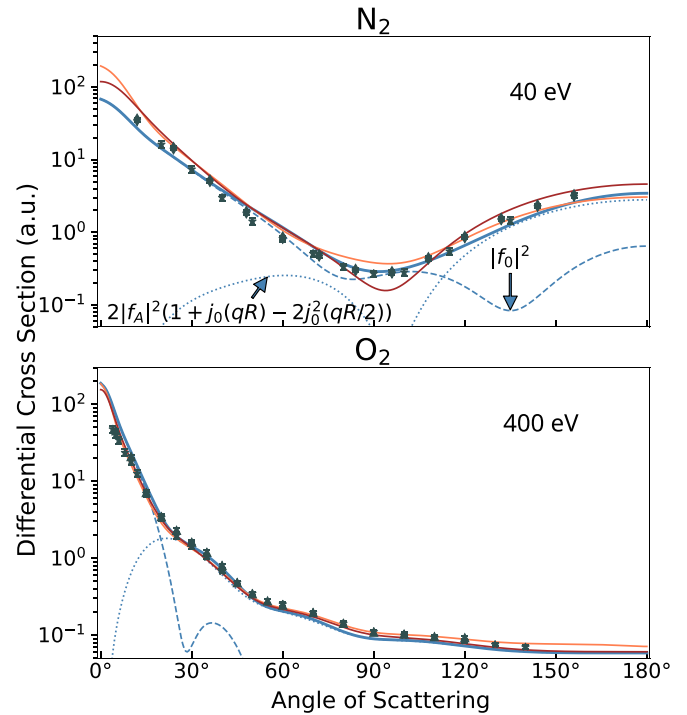


FIG. 6. Illustration of the present model (blue) compared with the screened independent atom model [29] (dark red) and higher-order multiple scattering IAM (orange). The dashed and dotted curves show how the contribution of $|f_0|^2$ (---) and $2|f_A|^2(1 + j_0(qR) - 2j_0^2(qR/2))$ (···) differ at low (40 eV) and high (400 eV) energies. Experimental data: N₂ - ★: Srivastava *et al.* [78]; ◇: Shyn and Carignan [79]; O₂ - ★: Daimon *et al.* [98]; △: Iga *et al.* [99].

model below 30 eV. First, a correct averaging of the potential harmonics is recommended: i.e., use (18) instead of (19). Second, the absorption potential requires some revision. Either a corrective factor should be used [54,100,101 Eq.(3), Eq.(12), Eqs.(1)-(3)] or a different energy threshold considered [55, §II.C]; otherwise a more elaborate model should be required. Third, more advanced calculations (coupled channels [25] and Schwinger variational [23, Eqs. (6)-(12)]), show in fact that accurate results can be obtained when yet another version of the absorption model [102, §3.2.3] is used, provided a completely different interpretation of the energy threshold E_{th} is taken [52,103, §II.B]. This implies that the coupling between different phase shifts due to the aspherical (multipole) components of the molecular potential become important below 30 eV. Another limitation of our method may come from the fact that we subtracted the zeroth interatomic interference term $j_0(qR/2)$ in (34) from the IAM according to first Born amplitudes \tilde{f} that does not rigorously apply to partial-wave amplitudes f . At high energies, this results in a slight overestimation of the present model at small scattering angles with respect to the IAM as seen in Fig. 6, bottom. The theory of multiple scattering shows that such overestimations can be corrected through inclusion of higher-order interference terms as conveyed by the orange curve on Fig. 6.

A notable exception is the case of H₂, which was tested down to our lowest limit value of 10 eV yielding reasonable agreement without requiring screening correction. This surprisingly good performance is due to the reduced internuclear

separation distance, giving a prominent role to the isotropic term of the molecular potential.

Regarding scattering at higher energies, since the molecule is represented as two unperturbed individual atoms, the energy threshold used in the quasifree absorption potential should rather be based on the atomic excitation threshold to stay consistent. The decomposition of our model enables one to use a different energy threshold for the molecular isotropic potential and the individual atomic potentials. This could potentially improve the consistency of the IAM throughout a large energy range and avoid to use corrective scaling factors as suggested in Staszewska *et al.* [101, Eqs. (1)-(2)] or Raj and Kumar [100] for O₂ specifically.

In light of the good overall agreement obtained, we suggest using our model's DCS for ordinary diatomic molecules down to 30 eV and for H₂ to 15 eV. They can provide a relatively simple way to build a database for predicting elastic scattering at intermediate energies in Monte Carlo electron collision simulations. For lower-energy scattering, the users can either resort to very accurate albeit somewhat costly computations [26,72,104] or to more semiempirical treatments [29,105,106].

In principle, the present methodology could include more realistic static potentials in the isotropic part arising from the molecular bond. Also, generalization for linear polyatomic molecules, notably CO₂ would not require significant effort. In this latter case, one would simply need to add the atomic potential of the middle carbon atom V_C into the averaged potential V_0 of Eq. (19), which would affect the calculated f_0 used in (34). In the future, this methodology could be tried upon more complex molecules for which the IAM is not satisfactory.

VII. SUMMARY AND CONCLUSIONS

Our calculations show that basic models relying upon a minimalist description of the optical potential are suitable for the generation of DCS databases for elastic scattering with diatomic molecules from intermediate to higher energies, where the experimental data is either outdated, sparse, incomplete, or controversial. The key points are summarized below.

(i) An averaged isotropic molecular potential can significantly improve the accuracy of differential cross sections calculated with the independent atom model.

(ii) A screening correction factor is essential to enhance the agreement of integrated cross sections at intermediate energies below 200 eV.

(iii) When using the quasifree semiempirical model for absorption of Staszewska *et al.* [107], better agreement is found for O₂ provided the excitation threshold E_{th} is identified with the first optically allowed transition.

(iv) Our model, without correlation and absorption, is particularly well suited to describe electron elastic scattering by H₂ due to its short internuclear separation.

ACKNOWLEDGMENTS

This work was supported by the European Research Council (ERC) under the European Union H2020 programme/ERC Grant Agreement No. 681257. The authors acknowledge financial support from the State Agency for

Research of the Spanish MCIU through the ‘‘Center of Excellence Severo Ochoa’’ award for the Instituto de Astrofísica de Andalucía (SEV-2017-0709), from the Regional Government of Andaluca (‘‘Junta de Andaluca’’) under grant PY20_00831, and from the European Research Council under the European Union’s Seventh Framework Programme (FP7/2007-2013)/ERC Grant Agreement No. 320839 and the Research Council of Norway under Contracts No. 208028/F50, 216872/F50 and No. 223252/F50 (CoE).

APPENDIX A: BORN APPROXIMATION APPLIED TO DECENTERED POTENTIALS

To show how the IAM is in fact a summation over Born partial amplitudes, let us first express a decentered central (atomic) potential V_A in terms of the Fourier transformed \tilde{V}_A :

$$V_A(r) = \frac{1}{(2\pi)^{3/2}} \int \tilde{V}_A(k) \exp(i\mathbf{k} \cdot \mathbf{r}) d^3\mathbf{k} \quad (\text{A1})$$

$$V_A\left(\mathbf{r} \pm \frac{\mathbf{R}}{2}\right) = \frac{1}{(2\pi)^{3/2}} \int \tilde{V}_A(k) \exp(i\mathbf{k} \cdot (\mathbf{r} \pm \mathbf{R}/2)) d^3\mathbf{k}, \quad (\text{A2})$$

$$V_A\left(\mathbf{r} \pm \frac{\mathbf{R}}{2}\right) = \frac{4\pi}{(2\pi)^{3/2}} \int \tilde{V}_A(k) \sum_l (\mp 1)^l j_l(kr) j_l\left(\frac{kR}{2}\right) \times (2l+1) P_l(\cos \chi) k^2 dk. \quad (\text{A3})$$

In (A3) we used a product of two Rayleigh expansions [108, §10.1.47]:

$$\exp(-i\mathbf{q} \cdot \mathbf{r}) = \sum_{l=0}^{\infty} (2l+1) (-i)^l j_l(qr) P_l(\cos(\hat{q}r)), \quad (\text{A4})$$

(where $\hat{q}r$ expresses the angle between \mathbf{q} and \mathbf{r}), the addition theorem [109, 14.30.9] and orthogonality [108, 14.30.8] of Legendre polynomials through spherical harmonics, with χ being the angle between \mathbf{r} and \mathbf{R} as in Fig. 1.

We recognize now through the Legendre polynomial $P_l(\cos \chi)$, the spherical-harmonic component V_{Al} of a decentered central potential as in (15). Replacing (A3) into the integral (25) for the Born scattered wave \tilde{f}_{Al} , we obtain:

$$\begin{aligned} \tilde{f}_{Al} &\equiv -2 \int r^2 j_l(qr) V_{Al}(r) dr \\ &= -2 \int r^2 j_l(qr) \frac{4\pi}{(2\pi)^{3/2}} \\ &\quad \times \int \tilde{V}_A(k) (\mp 1)^l j_l(kr) j_l(kR/2) (2l+1) k^2 dk dr. \end{aligned} \quad (\text{A5})$$

Applying the identity [109, 1.17.14]:

$$\int r^2 j_l(kr) j_l(qr) dr = \frac{\pi}{2q^2} [\delta(k-q) + (-1)^l \delta(k+q)] \quad (\text{A6})$$

we can swap in (A5) the integrals on dk and dr . Then using (A6) for the dr integration, we have:

$$\begin{aligned}\tilde{f}_{Al} &= -2 \frac{2\pi^2}{(2\pi)^{3/2}} \tilde{V}_A(q) (\mp 1)^l j_l(qR/2) (2l+1) \\ &= (\mp 1)^l (2l+1) j_l(qR/2) \frac{-2}{4\pi} \int V_A(r) e^{-i\mathbf{q}\cdot\mathbf{r}} d^3\mathbf{r} \\ &= (\mp 1)^l (2l+1) j_l(qR/2) \tilde{f}_A.\end{aligned}\quad (\text{A7})$$

Replacing this into Born's expression (24), in addition to the polarization V_p (which appears only for the isotropic $l=0$ term), the combination of IAM with Born's approximation for vibrationally elastic scattering gives:

$$\begin{aligned}\frac{d\sigma}{d\Omega} &= \sum_{l=0}^{\infty} \frac{1}{2l+1} \left| -2 \int r^2 j_l(qr) (V_{Al}(r) \right. \\ &\quad \left. + V_{A'l}(r) + \delta_{l0} V_p(r)) dr \right|^2 \\ &= \sum_{l=0}^{\infty} \frac{1}{2l+1} \left| (2l+1) j_l(qR/2) (\tilde{f}_A + (-1)^l \tilde{f}_{A'}) + \delta_{l0} \tilde{f}_M \right|^2 \\ &= \sum_{l=0}^{\infty} (2l+1) j_l^2\left(\frac{qR}{2}\right) |\tilde{f}_A + (-1)^l \tilde{f}_{A'}|^2 \\ &\quad + 2\text{Re}[\tilde{f}_M^* (\tilde{f}_A + \tilde{f}_{A'})] j_0\left(\frac{qR}{2}\right) + |\tilde{f}_M|^2 \\ &= |\tilde{f}_A|^2 + |\tilde{f}_{A'}|^2 + |\tilde{f}_M|^2 + 2\text{Re}[\tilde{f}_A \tilde{f}_{A'}^*] \frac{\sin(qR)}{qR} \\ &\quad + 2\text{Re}[\tilde{f}_M^* (\tilde{f}_A + \tilde{f}_{A'})] \frac{\sin(qR/2)}{qR/2}\end{aligned}\quad (\text{A8})$$

The infinite summation on the product of spherical Bessel functions comes from their addition theorem [108, §10.1.45, p.440]:

$$\sum_{l=0}^{\infty} (2l+1) j_l^2\left(\frac{qR}{2}\right) (\pm 1)^l = \begin{cases} 1 \\ \sin(qR)/qR \equiv j_0(qR) \end{cases}.\quad (\text{A9})$$

The result obtained (A8) corresponds to the zero-order expansion in the multiple scattering theory of Hayashi and Kuchitsu [59, Eq. (15), 18&31]. Noting in fact that $V_0 \equiv V_{A0} + V_{A'0} + V_p$ as in (16), we can now group the terms in (A8) differently and separate the $l=0$ term:

$$\begin{aligned}\frac{d\sigma}{d\Omega} &= \left| -2 \int r^2 j_0(qr) V_0(r) dr \right|^2 \\ &\quad + \sum_{l=1}^{\infty} \frac{1}{2l+1} \left| -2 \int r^2 j_l(qr) (V_{Al}(r) + V_{A'l}(r)) dr \right|^2\end{aligned}$$

Static molecular:

$$\tilde{f}_0 = (\tilde{f}_A + \tilde{f}_{A'}) j_0(qR/2) = (\tilde{f}_A + \tilde{f}_{A'}) \frac{\sin(qR/2)}{qR/2}\quad (\text{B5})$$

$$\begin{aligned}&= |\tilde{f}_0|^2 + \sum_{l=1}^{\infty} (2l+1) j_l^2\left(\frac{qR}{2}\right) |\tilde{f}_A + (-1)^l \tilde{f}_{A'}|^2 \\ &= |\tilde{f}_0|^2 - j_0^2\left(\frac{qR}{2}\right) |\tilde{f}_A + \tilde{f}_{A'}|^2 \\ &\quad + \left(|\tilde{f}_A|^2 + |\tilde{f}_{A'}|^2 + 2\text{Re}[\tilde{f}_A \tilde{f}_{A'}^*] \frac{\sin(qR)}{qR} \right).\end{aligned}\quad (\text{A10})$$

We have now uncovered a formula that explicitly links the IAM to a decomposition of anisotropic terms \tilde{f}_l from Born's first-order approximation. In particular, we can relate the first isotropic term $|\tilde{f}_0|^2$ in (A10) to the interferences of a molecular term \tilde{f}_M with atomic terms \tilde{f}_A and $\tilde{f}_{A'}$ in (A8) and their first harmonic $j_0(\frac{qR}{2})^2$ interatomic interference.

APPENDIX B: ANALYTICAL BORN AMPLITUDES AND PHASES

For the simple potentials presented: Yukawa static (6) and Buckingham polarization (9), the first Born integrals for the amplitude (4) and the phase-shifts (30) can be computed analytically [110, see 6.623(1), 6.612(3) for Yukawa and 6.565(3), 6.541(1-2) for Buckingham]:

Static atomic:

$$\tilde{f}_A = -2Z \int_0^{\infty} - \sum_{i=1}^{N_Y} \gamma_i \frac{e^{-\lambda_i r}}{r} j_0(qr) r^2 dr = \sum_{i=1}^{N_Y} \frac{2Z\gamma_i}{q^2 + \lambda_i^2}\quad (\text{B1})$$

$$\begin{aligned}\delta_{Al} &= -2k \int_0^{\infty} -Z \sum_{i=1}^{N_Y} \gamma_i \frac{e^{-\lambda_i r}}{r} j_l^2(kr) r^2 dr \\ &= \frac{Z}{k} \sum_{i=1}^{N_Y} \gamma_i Q_l \left(1 + \frac{\lambda_i^2}{2k^2} \right)\end{aligned}\quad (\text{B2})$$

Polarization:

$$\tilde{f}_B = -2 \int_0^{\infty} - \frac{\alpha_0 j_0(qr) r^2}{2(r^2 + r_c^2)^2} dr = \frac{\alpha_0 \pi}{4r_c} \exp(-qr_c)\quad (\text{B3})$$

$$\begin{aligned}\delta_{B\ell} &= -2k \int_0^{\infty} - \frac{\alpha_0 j_\ell^2(kr) r^2}{2(r^2 + r_c^2)^2} dr \\ &= \frac{\alpha_0 \pi}{2r_c} \left(I_{\ell+\frac{1}{2}}(kr_c) K'_{\ell+\frac{1}{2}}(kr_c) + \frac{1}{2kr_c} \right).\end{aligned}\quad (\text{B4})$$

The functions introduced are the Legendre function [108, Chap. 8] of the second kind Q_ℓ , the modified Bessel functions [108, Chap. 9] of the first $I_{\ell+\frac{1}{2}}$ and second $K_{\ell+\frac{1}{2}}$ kind.

The static molecular terms arise from integrals (4) and (30) with V taken as the static spherically averaged potential V_{s0} (20). For the phase shift, however, the integral has to be partly calculated by numerical quadrature. We give two variants in (B6) based on the partial-wave order ℓ and the magnitude of $\lambda_i R/2$.

$$\begin{aligned}
\tilde{\delta}_{M\ell} &= -2k \sum_{A,A'} (-Z) \sum_{i=1}^{N_y} \gamma_i \left(\int_0^{\frac{R}{2}} \frac{e^{-\lambda_i R/2} \sinh(\lambda_i r)}{R/2} \frac{j_\ell^2(kr) r^2 dr}{\lambda_i r} + \int_{\frac{R}{2}}^\infty \frac{e^{-\lambda_i r} \sinh(\lambda_i R/2)}{r} \frac{j_\ell^2(kr) r^2 dr}{\lambda_i R/2} \right) \\
&= 2k \sum_{A,A'} Z \sum_{i=1}^{N_y} \gamma_i \left\{ \frac{\sinh(\lambda_i R/2)}{\lambda_i R/2} \left(\int_0^{\frac{R}{2}} \frac{\sinh(\lambda_i (r - \frac{R}{2}))}{\sinh(\lambda_i \frac{R}{2})} j_\ell^2(kr) r^2 dr + \frac{1}{2} Q_\ell \left(1 + \frac{\lambda_i^2}{2k^2} \right) \right); \quad \lambda_i R/2 \lesssim 1, \ell \gg 1 \right. \\
&\quad \left. \frac{1}{\lambda_i R} \left(\int_0^\infty e^{-\lambda_i |r - R/2|} j_\ell^2(kr) r^2 dr - \frac{e^{-\lambda_i R/2}}{2} Q_\ell \left(1 + \frac{\lambda_i^2}{2k^2} \right) \right); \quad \lambda_i R/2 > 1, \ell \approx 1 \right.
\end{aligned} \tag{B6}$$

The integrals over V_{ex} and V_{abs} , would have to be computed by numerical quadrature.

-
- [1] S. Biagi, Monte Carlo simulation of electron drift and diffusion in counting gases under the influence of electric and magnetic fields, *Nucl. Instrum. Methods Phys. Res., Sect. A* **421**, 234 (1999).
- [2] C. Jackman and A. Green, Electron impact on atmospheric gases, 3. Spatial yield spectra for N_2 , *J. Geophys. Res.: Space Phys.* **84**, 2715 (1979).
- [3] V. Vahedi and M. Surendra, A Monte Carlo collision model for the particle-in-cell method: applications to argon and oxygen discharges, *Comput. Phys. Commun.* **87**, 179 (1995), Particle Simulation Methods.
- [4] D. C. Tyte, Carbon dioxide lasers, in *Advances in Quantum Electronics* (Academic Press, New York, 1970), P. 129.
- [5] O. Chanrion and T. Neubert, Production of runaway electrons by negative streamer discharges, *J. Geophys. Res.: Space Phys.* **115**, A00E32 (2010).
- [6] M. J. Brunger and S. J. Buckman, Electron-molecule scattering cross-sections. I. Experimental techniques and data for diatomic molecules, *Phys. Rep.* **357**, 215 (2002).
- [7] L. G. Christophorou and J. K. Olthoff, *Electron-Molecule Interactions in the Gas Phase: Cross Sections and Coefficients* (Springer US, Boston, 2004), Chap. 2, pp. 61–111.
- [8] S. Trajmar and D. F. Register, *Experimental Techniques for Cross-Section Measurements* (Springer US, Boston, 1984), pp. 427–493.
- [9] B. D. Buckley, P. G. Burke, and C. J. Noble, *Computational Methods for Low-Energy Electron-Molecule Collisions* (Springer US, Boston, 1984), pp. 495–556.
- [10] F. Gianturco and A. Jain, The theory of electron scattering from polyatomic molecules, *Phys. Rep.* **143**, 347 (1986).
- [11] N. F. Lane, The theory of electron-molecule collisions, *Rev. Mod. Phys.* **52**, 29 (1980).
- [12] T. Rescigno, V. McKoy, and B. Schneider, *Electron-Molecule and Photon-Molecule Collisions* (Springer, Boston, 1979).
- [13] A. Jablonski, F. Salvat, C. J. Powell, and A. Y. Lee, Nist electron elastic-scattering cross-section database version 4.0, NIST Standard Reference Database Number 64, 2016, URL <https://srdata.nist.gov/srd64/>, consulted Nov 2021.
- [14] S. Pancheshnyi, M. Bordage, B. Chaudhury, S. Chowdhury, G. Hagelaar, L. Pitchford, V. Puech, K. Bartschat, W. Morgan, L. Viehland, O. Zatsarinny, J. d’Urquijo, A. Castrejón-Pita, J. Hernández-Ávila, E. Basurto, I. Bray, D. Fursa, S. Biagi, Quantemol, L. Alves, C. Ferreira, I. Kochetov, A. Napartovich, Y. Itikawa, A. Stauffer, C. Brion, J. van Dijk, W. Graef, M. Hopkins, B. Yee, D. Mihailova, E. Carbone, and J. Stephens, Lxcat, French National Center for Scientific Research, 2010, <https://www.lxcat.net/>.
- [15] F. Salvat, A. Jablonski, and C. J. Powell, ELSEPA-Dirac partial-wave calculation of elastic scattering of electrons and positrons by atoms, positive ions and molecules, *Comput. Phys. Commun.* **165**, 157 (2005).
- [16] F. Salvat, A. Jablonski, and C. J. Powell, ELSEPA-Dirac partial-wave calculation of elastic scattering of electrons and positrons by atoms, positive ions and molecules (new version announcement), *Comput. Phys. Commun.* **261**, 107704 (2021).
- [17] L. A. Morgan, J. Tennyson, and C. J. Gillan, The UK molecular R-matrix codes, *Comput. Phys. Commun.* **114**, 120 (1998).
- [18] L. G. Christophorou and J. K. Olthoff, *Synthesis and Assessment of Electron Collision Data* (Springer US, Boston, 2004), Chap. 3, pp. 113–134.
- [19] I. Iga, I. Sanches, E. de Almeida, R. Sugohara, L. Rosani, and M.-T. Lee, Experimental verification on the applicability of the independent-atom model (IAM) for elastic electron-molecule scattering in the intermediate-energy range, *J. Electron Spectrosc. Relat. Phenom.* **155**, 7 (2007), Scattering, Coincidence and Absorption Studies of Molecules.
- [20] J. Tennyson, D. B. Brown, J. J. Munro, I. Rozum, H. N. Varambhia, and N. Vinci, Quantemol-N: an expert system for performing electron molecule collision calculations using the R-matrix method, *J. Phys.: Conf. Ser.* **86**, 012001 (2007).
- [21] B. Cooper, M. Tudorovskaya, S. Mohr, A. O’Hare, M. Hanicinea, A. Dzarasova, J. D. Gorfinkiel, J. Benda, Z. Mašín, A. F. Al-Refaie, P. J. Knowles, and J. Tennyson, Quantemol electron collisions (QEC): An enhanced expert system for performing electron molecule collision calculations using the R-matrix method, *Atoms* **7**, 97 (2019).
- [22] I. Iga, M.-T. Lee, and R. Bonham, Role of the intramolecular multiple scattering on electron diffraction from nitrogen molecule in the intermediate energy range, *J. Mol. Struct. (THEOCHEM)* **468**, 241 (1999).
- [23] M.-T. Lee and I. Iga, Elastic and total cross sections for electron scattering by nitrogen molecule in the intermediate energy range, *J. Phys. B: At., Mol. Opt. Phys.* **32**, 453 (1999).
- [24] H. Kutz and H.-D. Meyer, Rotational excitation of N_2 and Cl_2 molecules by electron impact in the energy range 0.01–1000 eV: Investigation of excitation mechanisms, *Phys. Rev. A* **51**, 3819 (1995).
- [25] M. A. Morrison and W. Sun, *How to Calculate Rotational and Vibrational Cross Sections for Low-Energy Electron Scattering from Diatomic Molecules using Close-Coupling Techniques* (Springer US, Boston, 1995), pp. 131–190.
- [26] W. Sun, M. A. Morrison, W. A. Isaacs, W. K. Trail, D. T. Alle, R. J. Gulley, M. J. Brennan, and S. J. Buckman, Detailed

- theoretical and experimental analysis of low-energy electron- N_2 scattering, *Phys. Rev. A* **52**, 1229 (1995).
- [27] K. Josphipura, Polarization and exchange in electron scattering by atoms in solids, *Solid State Commun.* **60**, 277 (1986).
- [28] F. Salvat, F. Mayol, E. Molins, and J. Parellada, A simple model for electron scattering: Elastic cross sections, *J. Phys. D* **18**, 1401 (1985).
- [29] F. Blanco and G. García, Screening corrections for calculation of electron scattering differential cross sections from polyatomic molecules, *Phys. Lett. A* **330**, 230 (2004).
- [30] K. N. Josphipura and P. M. Patel, Electron impact total (elastic + inelastic) cross-sections of C, N & O atoms and their simple molecules, *Z. Phys. D: At., Mol. Clusters* **29**, 269 (1994).
- [31] M. H. Khandker, N. T. Arony, A. K. F. Haque, M. Maaza, M. M. Billah, and M. A. Uddin, Scattering of e^\pm from N_2 in the energy range 1 eV-10 keV, *Mol. Phys.* **118**, e1699183 (2020).
- [32] K. Onda and D. G. Truhlar, New approaches to the quantum-mechanical treatment of charge polarization in intermediate-energy electron scattering, *Phys. Rev. A* **22**, 86 (1980).
- [33] M. E. Riley and D. G. Truhlar, Approximations for the exchange potential in electron scattering, *J. Chem. Phys.* **63**, 2182 (1975).
- [34] F. Salvat, J. D. Martinez, R. Mayol, and J. Parellada, Analytical Dirac-Hartree-Fock-Slater screening function for atoms ($Z=1-92$), *Phys. Rev. A* **36**, 467 (1987).
- [35] G. Staszewska, D. W. Schwenke, D. Thirumalai, and D. G. Truhlar, Quasifree-scattering model for the imaginary part of the optical potential for electron scattering, *Phys. Rev. A* **28**, 2740 (1983).
- [36] L. F. Canto and M. S. Hussein, *Approximate Methods in Potential Scattering* (World Scientific, Singapore, 2013), Chap. 2, pp. 161–166.
- [37] K. Takayanagi, Scattering of slow electrons by molecules, *Prog. Theor. Phys. Suppl.* **40**, 216 (1967).
- [38] R. G. Newton, *Cross Sections* (Springer, Berlin, 1982), Chap. 8, pp. 211–227.
- [39] L. F. Canto and M. S. Hussein, *Green's Functions, T- and S-Matrices* (World Scientific, Singapore, 2013), Chap. 4, pp. 107–156.
- [40] K. Takayanagi and Y. Itikawa, The rotational excitation of molecules by slow electrons, *Adv. At. Mol. Phys.* **6**, 105 (1970).
- [41] D. M. Chase, Adiabatic approximation for scattering processes, *Phys. Rev.* **104**, 838 (1956).
- [42] M. A. Morrison, A. N. Feldt, and D. Austin, Adiabatic approximations for the nuclear excitation of molecules by low-energy electron impact: Rotational excitation of H_2 , *Phys. Rev. A* **29**, 2518 (1984).
- [43] M. Fink and R. A. Bonham, *Electrostatic Potential of Free Molecules Derived from Electron Diffraction Results* (Springer US, Boston, 1981), pp. 93–121.
- [44] P. Politzer, *Relationships between the Energies of Atoms and Molecules and the Electrostatic Potentials at Their Nuclei* (Springer US, Boston, 1981), pp. 7–28.
- [45] K. Takayanagi, *Introduction to Electron-Molecule Collisions* (Springer US, Boston, 1984), pp. 1–87.
- [46] P. Carsky and R. Curik, *Low-Energy Electron Scattering from Molecules, Biomolecules and Surfaces* (CRC Press, Boca Raton, 2012).
- [47] F. Gianturco and J. Rodriguez-Ruiz, Correlation forces in electron scattering from atoms and molecules: a density functional approach, *J. Mol. Struct. (THEOCHEM)* **260**, 99 (1992).
- [48] B. Bransden and M. McDowell, Electron scattering by atoms at intermediate energies: I. Theoretical models, *Phys. Rep.* **30**, 207 (1977).
- [49] J. B. Furness and I. E. McCarthy, Semiphenomenological optical model for electron scattering on atoms, *J. Phys. B* **6**, 2280 (1973).
- [50] R. J. Drachman, Asymptotic effective potentials for electron-hydrogen scattering, *J. Phys. B* **12**, L699 (1979).
- [51] K. Onda, Electronic polarization of atoms in charged-particle impact, Technical Report 471, Institute for Space and Aeronautical Science, University of Tokyo, 1971.
- [52] A. Jain and K. L. Baluja, Total (elastic plus inelastic) cross sections for electron scattering from diatomic and polyatomic molecules at 10–5000 eV: H_2 , Li_2 , HF, CH_4 , N_2 , CO, C_2H_2 , HCN, O_2 , HCl, H_2S , PH_3 , SiH_4 , and CO_2 , *Phys. Rev. A* **45**, 202 (1992).
- [53] G. Staszewska, P. Staszewski, and K. Żebrowski, Local effective polarization and absorption potentials from cross-sections for e-atom scattering, *Phys. Lett. A* **372**, 6925 (2008).
- [54] F. Salvat, Optical-model potential for electron and positron elastic scattering by atoms, *Phys. Rev. A* **68**, 012708 (2003).
- [55] F. Blanco and G. García, Improvements on the quasifree absorption model for electron scattering, *Phys. Rev. A* **67**, 022701 (2003).
- [56] H. H. Magnus, W. F. Oberhettinger, and R. P. Soni, Bessel functions, *Formulas and Theorems for the Special Functions of Mathematical Physics* (Springer Berlin Heidelberg, 1966), Chap. 3, pp. 65–151.
- [57] S. Trajmar, D. Register, and A. Chutjian, Electron scattering by molecules II. Experimental methods and data, *Phys. Rep.* **97**, 219 (1983).
- [58] L. F. Canto and M. S. Hussein, *The Partial Wave Expansion Method* (World Scientific, Singapore, 2013), Chap. 2, pp. 41–78.
- [59] S. Hayashi and K. Kuchitsu, Elastic scattering of electrons by molecules at intermediate energies. I. General theory, *J. Phys. Soc. Jpn.* **41**, 1724 (1976).
- [60] N. Mott and H. S. W. Massey, *The Theory of Atomic Collisions*, 3rd ed. (Clarendon Press, Oxford, 1965).
- [61] Edited by F. Calogero, 3 Derivation of the phase equation, Mathematics in Science and Engineering, Variable Phase Approach to Potential Scattering, Vol. 35 (Elsevier, Amsterdam, 1967). Careful about the notation for $V(r)$, it includes already the factor 2 issued by the kinetic operator in the traditional Hartree atomic units.
- [62] D. A. Kohl and M. M. Arvedson, Elastic electron scattering. I. Scattering from diatomic potentials, *J. Chem. Phys.* **72**, 1915 (1980).
- [63] Y. Jiang, J. Sun, and L. Wan, Geometric shielding effects of electron scattering from polyatomic molecules, *Phys. Lett. A* **237**, 53 (1997).
- [64] A. Zecca, R. Melissa, R. S. Brusa, and G. P. Karwasz, Additivity rule for electron-molecule cross section calculation: A geometrical approach, *Phys. Lett. A* **257**, 75 (1999).

- [65] F. Blanco and G. García, Screening corrections for calculation of electron scattering from polyatomic molecules, *Phys. Lett. A* **317**, 458 (2003).
- [66] H. L. Cox and R. A. Bonham, Elastic electron scattering amplitudes for neutral atoms calculated using the partial wave method at 10, 40, 70, and 100 kV for $Z = 1$ to $Z = 54$, *J. Chem. Phys.* **47**, 2599 (1967).
- [67] F. A. Gianturco and S. Scialla, Local approximations of exchange interaction in electron-molecule collisions: the methane molecule, *J. Phys. B* **20**, 3171 (1987).
- [68] J. P. Perdew and A. Zunger, Self-interaction correction to density-functional approximations for many-electron systems, *Phys. Rev. B* **23**, 5048 (1981).
- [69] S. V. Khristenko, V. P. Shevelko, and A. I. Maslov, *Collisions of Molecules with Electrons* (Springer, Berlin, 1998), pp. 122–174.
- [70] G. G. Raju, *Gaseous Electronics: Tables, Atoms, and Molecules* (CRC Press, Boca Raton 2012).
- [71] P. Baille and J. W. Darewych, Comparison of local exchange potentials for electron scattering by hydrogen molecules, *J. Phys. B* **10**, L615 (1977).
- [72] A. Klonover and U. Kaldor, Ab initio electron-molecule scattering theory including polarisation: elastic scattering and rotational excitation of H_2 , *J. Phys. B* **11**, 1623 (1978).
- [73] S. K. Srivastava, A. Chutjian, and S. Trajmar, Absolute elastic differential electron scattering cross sections in the intermediate energy region. I. H_2 , *J. Chem. Phys.* **63**, 2659 (1975).
- [74] T. W. Shyn and W. E. Sharp, Angular distributions of electrons elastically scattered from H_2 , *Phys. Rev. A* **24**, 1734 (1981).
- [75] M. A. Khakoo and S. Trajmar, Elastic electron scattering cross sections for molecular hydrogen, *Phys. Rev. A* **34**, 138 (1986).
- [76] J. Muse, H. Silva, M. C. A. Lopes, and M. A. Khakoo, Low energy elastic scattering of electrons from H_2 and N_2 , *J. Phys. B: At., Mol. Opt. Phys.* **41**, 095203 (2008).
- [77] B. van Wingerden, F. J. de Heer, E. Weigold, and K. J. Nygaard, Elastic scattering of electrons by molecular and atomic hydrogen, *J. Phys. B* **10**, 1345 (1977).
- [78] S. K. Srivastava, A. Chutjian, and S. Trajmar, Absolute elastic differential electron scattering cross sections in the intermediate energy region. II. N_2 , *J. Chem. Phys.* **64**, 1340 (1976).
- [79] T. W. Shyn and G. R. Carignan, Angular distribution of electrons elastically scattered from gases: 1.5–400 eV on N_2 , II, *Phys. Rev. A* **22**, 923 (1980).
- [80] R. D. DuBois and M. E. Rudd, Differential cross sections for elastic scattering of electrons from argon, neon, nitrogen and carbon monoxide, *J. Phys. B* **9**, 2657 (1976).
- [81] D. Herrmann, K. Jost, J. Kessler, and M. Fink, Differential cross sections for elastic electron scattering. II. Charge cloud polarization in N_2 , *J. Chem. Phys.* **64**, 1 (1976).
- [82] T. W. Shyn, W. E. Sharp, Angular distribution of electrons elastically scattered from O_2 : 2.0–200-V impact energy, *Phys. Rev. A* **26**, 1369 (1982).
- [83] P. H. Krupenie, The spectrum of molecular oxygen, *J. Phys. Chem. Ref. Data* **1**, 423 (1972).
- [84] K. Wakiya, Differential and integral cross sections for the electron impact excitation of O_2 . I. Optically allowed transitions from the ground state, *J. Phys. B* **11**, 3913 (1978).
- [85] A. V. Phelps and L. C. Pitchford, Anisotropic scattering of electrons by N_2 and its effect on electron transport, *Phys. Rev. A* **31**, 2932 (1985).
- [86] Y. Itikawa, Cross sections for electron collisions with nitrogen molecules, *J. Phys. Chem. Ref. Data* **35**, 31 (2006).
- [87] Y. Itikawa, Cross sections for electron collisions with oxygen molecules, *J. Phys. Chem. Ref. Data* **38**, 1 (2009).
- [88] J.-S. Yoon, M.-Y. Song, J.-M. Han, S. H. Hwang, W.-S. Chang, B. Lee, and Y. Itikawa, Cross sections for electron collisions with hydrogen molecules, *J. Phys. Chem. Ref. Data* **37**, 913 (2008).
- [89] S. Altshuler, Theory of low-energy electron scattering by polar molecules, *Phys. Rev.* **107**, 114 (1957).
- [90] H. Tanaka, S. K. Srivastava, and A. Chutjian, Absolute elastic differential electron scattering cross sections in the intermediate energy region. IV. CO, *J. Chem. Phys.* **69**, 5329 (1978).
- [91] B. Mojarrabi, R. J. Gulley, A. G. Middleton, D. C. Cartwright, P. J. O. Teubner, S. J. Buckman, and M. J. Brunger, Electron collisions with NO: elastic scattering and rovibrational (0 to 1, 2, 3, 4) excitation cross sections, *J. Phys. B: At., Mol. Opt. Phys.* **28**, 487 (1995).
- [92] B. H. Choi, R. T. Poe, J. C. Sun, and Y. Shan, Two-potential approach for electron-molecular collisions at intermediate and high energies; application to e - N_2 scatterings, *Phys. Rev. A* **19**, 116 (1979).
- [93] A. Jain and S. S. Tayal, Modified-independent-atom-model (MIAM) calculations for e - CO_2 elastic scattering at 50–500 eV, *J. Phys. B* **15**, L867 (1982).
- [94] M.-T. Lee and L. C. G. Freitas, Incoherent renormalised multicentre potential model for elastic scattering of electrons by linear molecules at intermediate and high energies, *J. Phys. B* **14**, 1053 (1981).
- [95] S. Hayashi and K. Kuchitsu, Elastic scattering of electrons by molecules at intermediate energies. calculation of double scattering effects in N_2 and P_4 , *Chem. Phys. Lett.* **41**, 575 (1976).
- [96] D. A. Kohl and M. M. Arvedson, Elastic electron scattering from molecular potentials, *J. Chem. Phys.* **73**, 3818 (1980).
- [97] S. S. Tayal, A. Jain, A. N. Tripathi, and M. K. Srivastava, Elastic scattering of electrons by N_2 , O_2 , and CO in the energy range 0.1–3 keV, *J. Chem. Phys.* **78**, 3021 (1983).
- [98] H. Daimon, S. Hayashi, T. Kondow, and K. Kuchitsu, Measurements of differential cross sections of low-energy electrons elastically scattered by gas molecules. II. Scattering of 200–500 eV electrons by molecular oxygen, *J. Phys. Soc. Jpn.* **51**, 2641 (1982).
- [99] I. Iga, L. Mu-Tao, J. C. Nogueira, and R. S. Barbieri, Elastic differential cross section measurements for electron scattering from Ar and O_2 in the intermediate-energy range, *J. Phys. B* **20**, 1095 (1987).
- [100] D. Raj and A. Kumar, Elastic scattering of electrons by molecular oxygen, *Phys. Lett. A* **282**, 284 (2001).
- [101] G. Staszewska, P. Staszewski, and K. Żebrowski, On an improved model of a complex optical potential for electron elastic scattering, *J. Electron Spectrosc. Relat. Phenom.* **168**, 40 (2008).
- [102] G. Staszewska, P. Staszewski, and K. Żebrowski, Effective non-empirical absorption potentials based on quasifree-scattering model, *J. Electron Spectrosc. Relat. Phenom.* **162**, 56 (2008).
- [103] M.-T. Lee, I. Iga, L. E. Machado, and L. M. Bescansin, Model absorption potential for electron-molecule scattering in the intermediate-energy range, *Phys. Rev. A* **62**, 062710 (2000).

- [104] I. Bray, I. B. Abdurakhmanov, J. J. Bailey, A. W. Bray, D. V. Fursa, A. S. Kadyrov, C. M. Rawlins, J. S. Savage, A. T. Stelbovics, and M. C. Zammit, Convergent close-coupling approach to light and heavy projectile scattering on atomic and molecular hydrogen, *J. Phys. B: At., Mol. Opt. Phys.* **50**, 202001 (2017).
- [105] Z. Idziaszek, P. Miszta, and G. Karwasz, Modified effective range theory for electron and positron scattering on nitrogen and carbon dioxide, *J. Phys.: Conf. Ser.* **194**, 052010 (2009).
- [106] A. Mann and F. Linder, Low-energy electron scattering from halomethanes. I. Elastic differential cross section for e-CF₄ scattering, *J. Phys. B: At., Mol. Opt. Phys.* **25**, 533 (1992).
- [107] G. Staszewska, D. W. Schwenke, and D. G. Truhlar, Investigation of the shape of the imaginary part of the optical-model potential for electron scattering by rare gases, *Phys. Rev. A* **29**, 3078 (1984).
- [108] M. Abramowitz and I. Stegun, *Handbook of Mathematical Functions: With Formulas, Graphs, and Mathematical Tables*, Applied Mathematics Series (Dover Publications, Mineola, 1965).
- [109] F. Olver, D. Lozier, R. Boisvert, and C. Clark, *The NIST Handbook of Mathematical Functions* (Cambridge University Press, New York, 2010).
- [110] I. Gradshteyn and I. Ryzhik, 6-7 - definite integrals of special functions, in *Table of Integrals, Series, and Products*, 8th edition (Academic Press, Boston, 2014), pp. 637–775.